Electronic Supplementary Material (ESI) for Energy Advances.

Supporting Information to

Fabrication of Nanocrystalline High-Entropy Oxide $CoNiFeCrMnO_x$ Thin Film Electrodes by Dip-Coating for Oxygen Evolution Electrocatalysis

Qingyang Wu[a], Achim Alkemper[a], Stefan Lauterbach[b], Jan P. Hofmann[a] and Marcus Einert[a,]*

[a] Surface Science Laboratory, Department of Materials and Earth Sciences, Technical University of Darmstadt, Otto-Berndt-Strasse 3, 64287 Darmstadt, Germany;

[b] Institute for Applied Geosciences, Geomaterial Science, Technical University of Darmstadt, Schnittspahnstrasse 9, 64287 Darmstadt, Germany

Corresponding Author

*E-mail: Dr. M. Einert: meinert@surface.tu-darmstadt.de

Phone: +49 6151 16-20770

Experimental Section

Materials. All chemicals were of analytical grade and used as-received: chromium(III) nitrate nonahydrate (≥99.99%, Sigma-Aldrich), manganese(II) nitrate hydrate (98%, Sigma-Aldrich), iron(II) nonahydrate (≥99.95%, Sigma-Aldrich), cobalt(II) nitrate hexahydrate (99.999%, Sigma-Aldrich), nickel(II) nitrate hexahydrate (99.999%, Sigma-Aldrich), H-$(C_2H_4O)_{100}$-$(C_3H_6O)_{65}$-$(C_2H_4O)_{100}$-H (Pluronic F-127, Sigma-Aldrich), 1 M KOH (Carl Roth), ethanol (EtOH, ≥99.8%, Carl Roth), and 2-methoxyethanol (2-ME, ≥99.5%, Sigma-Aldrich).

Synthesis of HEO Thin Films. For the synthesis of the dip-coating solution according to literature,[1] 45 mg of Pluronic F-127 was dissolved 1.4 mL of 2-ME and 96 mg of $Cr(NO_3)_3 \cdot 9\ H_2O$, whereas for the metal precursors 60 mg of $Mn(NO_3)_2 \cdot x\ H_2O$, 97 mg of $Fe(NO_3)_3 \cdot 9\ H_2O$, 70 mg of $Co(NO_3)_2 \cdot 6\ H_2O$, and 70mg of $Ni(NO_3)_2 \cdot 6\ H_2O$ were dissolved in 0.8 mL of EtOH. Both solutions were stirred separately with a magnetic stirrer for 1 h until a homogeneous solution was received. Afterwards, both solutions were mixed dropwise and stirred for an hour. All substrates were cleaned in ethanol and acetone in an ultrasonication bath each for 15 min. Fluorine-doped SnO_2 (FTO) and silicon (100) wafers were utilized as substrates and immersed into the dip-coating solution. Optimum dip-coating conditions were found between 13−16% relative humidity and applying a constant withdrawal speed of 4−8 mm/s. Subsequently, the samples were directly transferred into a pre-heated (125 °C) muffle furnace (Nabertherm LT3/11) and heated to 400°C (with a heating ramp of 5°C/min) and kept at this temperature for either 10 min or 1 h.

Structural Characterization. Scanning electron microscopy (SEM) images were obtained on a Philips XL30 FEG at an acceleration voltage of 30 keV and a working distance of about 4 cm. GIWAXS was carried out on a D8 Advance diffractometer from Bruker (Cu Kα radiation) equipped with a Sol-X detector. Data were collected in Bragg−Brentano geometry between 10 and 60° (in units of 2θ) using a step size 0.01°. The film thicknesses were collected with a Bruker profilometer (Dektak XT) using a stylus force of 3 mg and a scan rate of 10 µm/s. Before conducting Transmission electron microscopy (TEM), some flakes of the HEO thin film were scraped off from silicon substrates. Afterwards, the flakes were dispersed in a small amount of ethanol and dispersed by the aid of ultrasonication. A droplet was deposited on a carbon-coated copper grid (holey type, Plano GmbH, Wetzlar) and dried. To avoid charging under the electron beam, the grid was coated with a thin carbon film (carbon coater MED 010, Bal-TecAG, Balzers, Liechtenstein). Samples were examined using an FEG TEM (JEM2100F, JEOL Ltd., Tokyo, Japan) in TEM and scanning transmission electron microscopy (STEM) mode. EDS maps were recorded utilizing an Oxford X-Max 80 EDS detector.

Spectroscopic characterization. XP spectra were acquired at beamline PM3 of BESSY II (Berlin, Germany) employing the SoLiAS endstation equipped with a Phoibos 150 analyzer, 1D-delay line detector and HSA3500 controller operated by the SpecsLab Prodigy software (SPECS GmbH, Germany). Data was recorded in fixed analyzer transmission mode with the binding energy scale calibrated against Ag $3d_{5/2}$ and Fermi level at 368.2 eV and 0.0 eV, respectively with an uncertainty of 0.1 eV. Possible sample charging effects could not be corrected for. Survey spectra were taken with a pass energy of 20 eV, step size of 0.5 eV and excitation energy of 1200 eV. Detail spectra were obtained at a pass energy of 10 eV employing a step size of 0.05 eV with a kinetic energy of the photoelectrons of 610 eV irrespective of the analyzed core level to prevent an overlap of Auger lines and enable a consistent probed depth.

Electrochemical Characterization. Electrochemical characterization of the samples was accomplished by a GAMRY Interface 1000E potentiostat using a three-electrode setup (Zahner cell PECC2) with a Hg/HgO reference electrode and a platinum wire as the counter electrode in 1 M KOH. Cyclic voltammetry (CV) was carried out between 1.0 and 1.6 V vs. reversible hydrogen electrode (RHE) with a scan rate of 100 mV/s and a step size of 1 mV. Linear sweep voltammetry (LSV) was conducted between 0.9 and 1.9 V vs RHE with a scan rate of 1 mV/s. iR correction of LSV curves was done by subtraction of the electrolyte resistance derived from impedance spectroscopy. Scan rate-dependent cyclic voltammetry was obtained by measuring fast potential sweep curves for scan rates of 10-80 mV/s and in a non-faradaic potential range between 0.8 and 1.0 V vs RHE. Differential current densities were obtained after the method of McCrory et al.[2] The obtained double-layer capacitance (C_{DL}) can be converted into the electrochemical surface area (ECSA) by $ECSA = \frac{C_{DL}}{C_S}$, with C_S the specific capacitance, which was taken from the literature[2] as the average value of 40 µF/cm^2. Electrochemical impedance spectroscopy (EIS) was measured at 1.6 eV vs. RHE between 100 kHz and 1 Hz with AC modulation of 10 mV and 25 points per decade. Chronopotentiometry (CP) was recorded at geometric current density of 10 mA/cm^2 for 7200 s without equilibration time. The transcription of the reference potential (of the Hg/HgO electrode) into the reversible hydrogen electrode (RHE) potential was given by the Nernst equation.

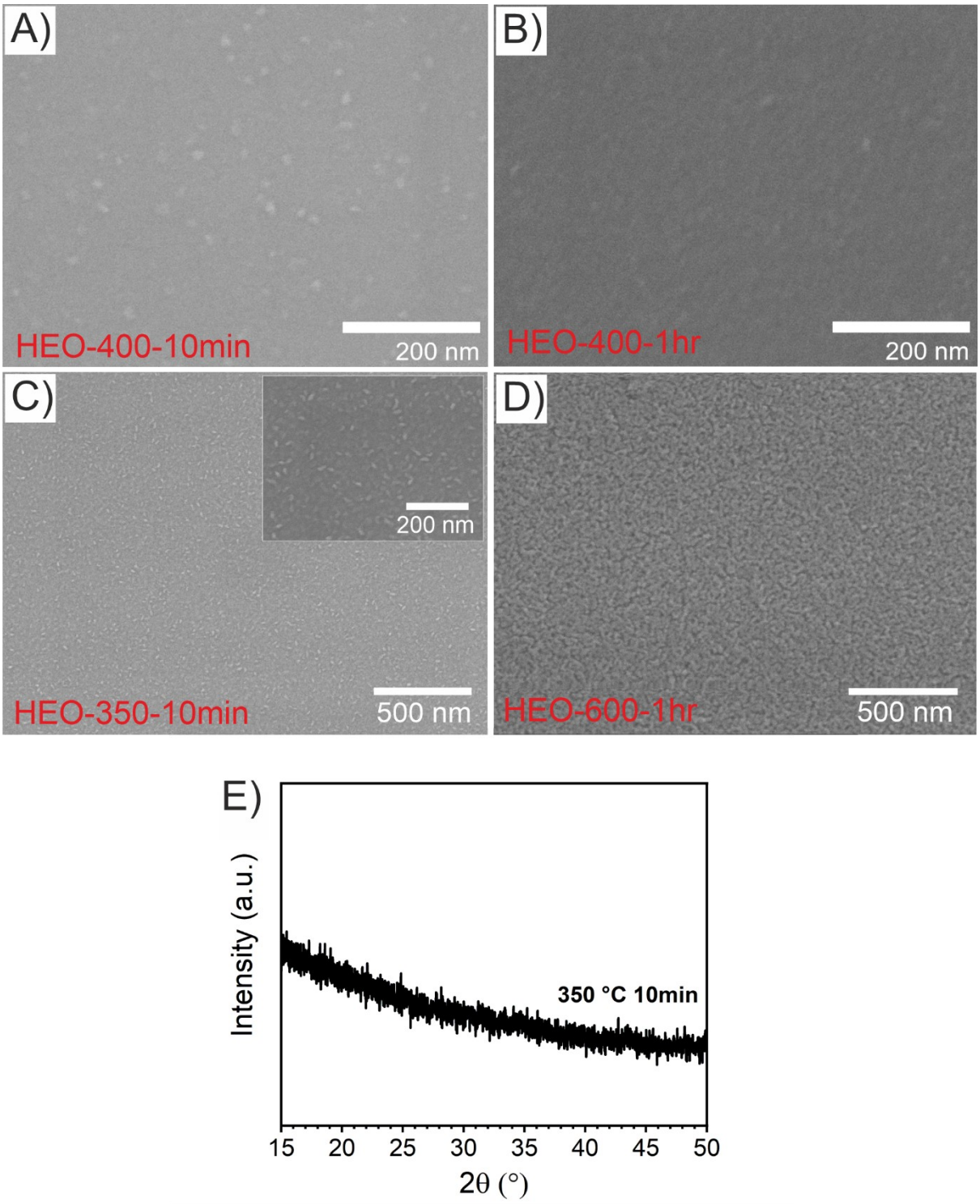

Figure S1. Top-view SEM images of A) HEO-400-10min, B) HEO-400-1h, C) HEO-350-10min and D) HEO-600-1hr thin films analyzed at high magnifications with 30 kV. E) XRD pattern of HEO-350-10-min showing an X-ray amorphous structure.

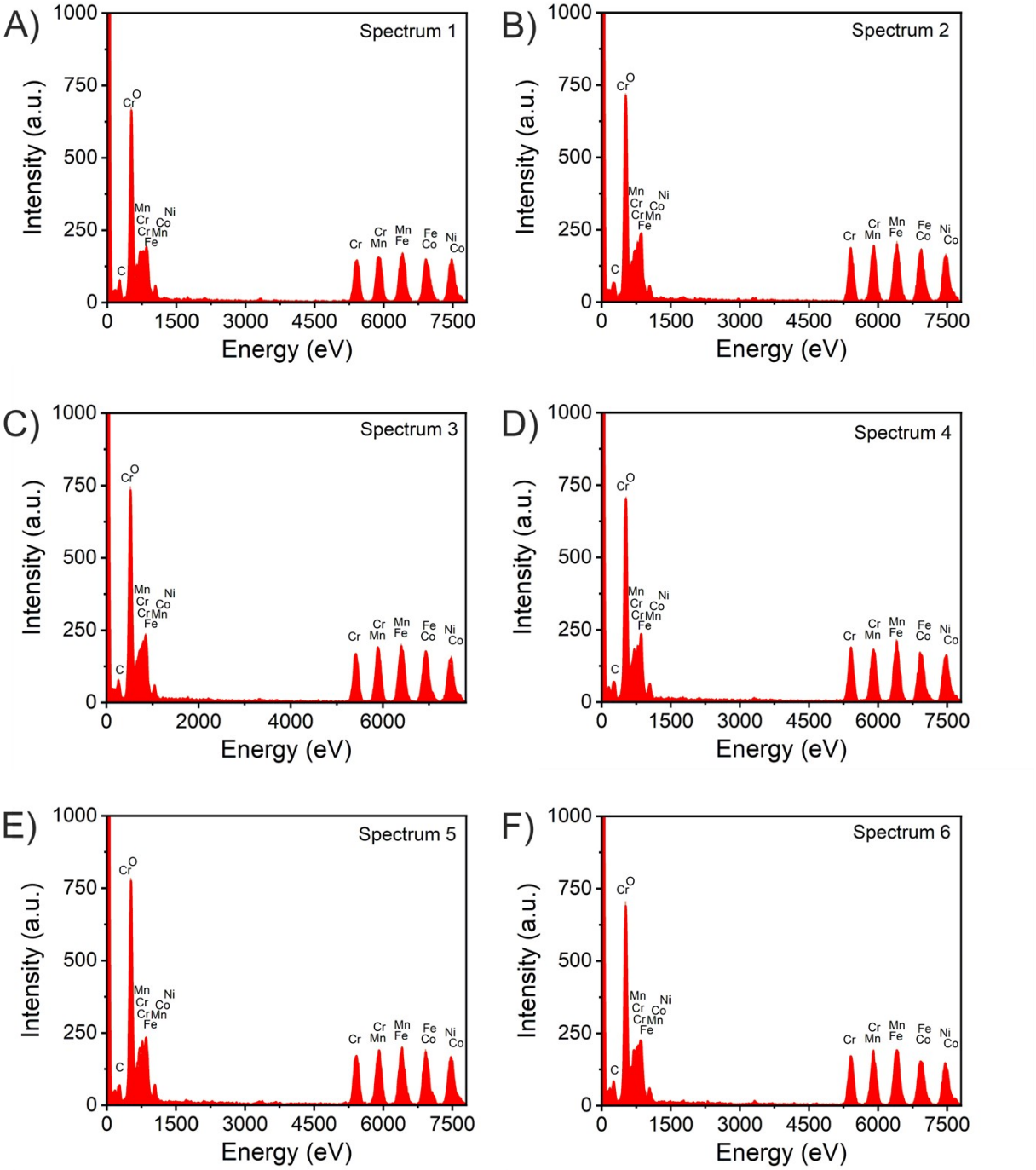

Figure S2. A)−F) STEM-based EDS spectra (1-6) conducted at six distinct spots of the HEO-400 thin films showing signals of all incorporated cations (Cr, Mn, Fe, Co, Ni) in near-equiatomic concentrations (± 5 % error) as well as carbon and oxygen.

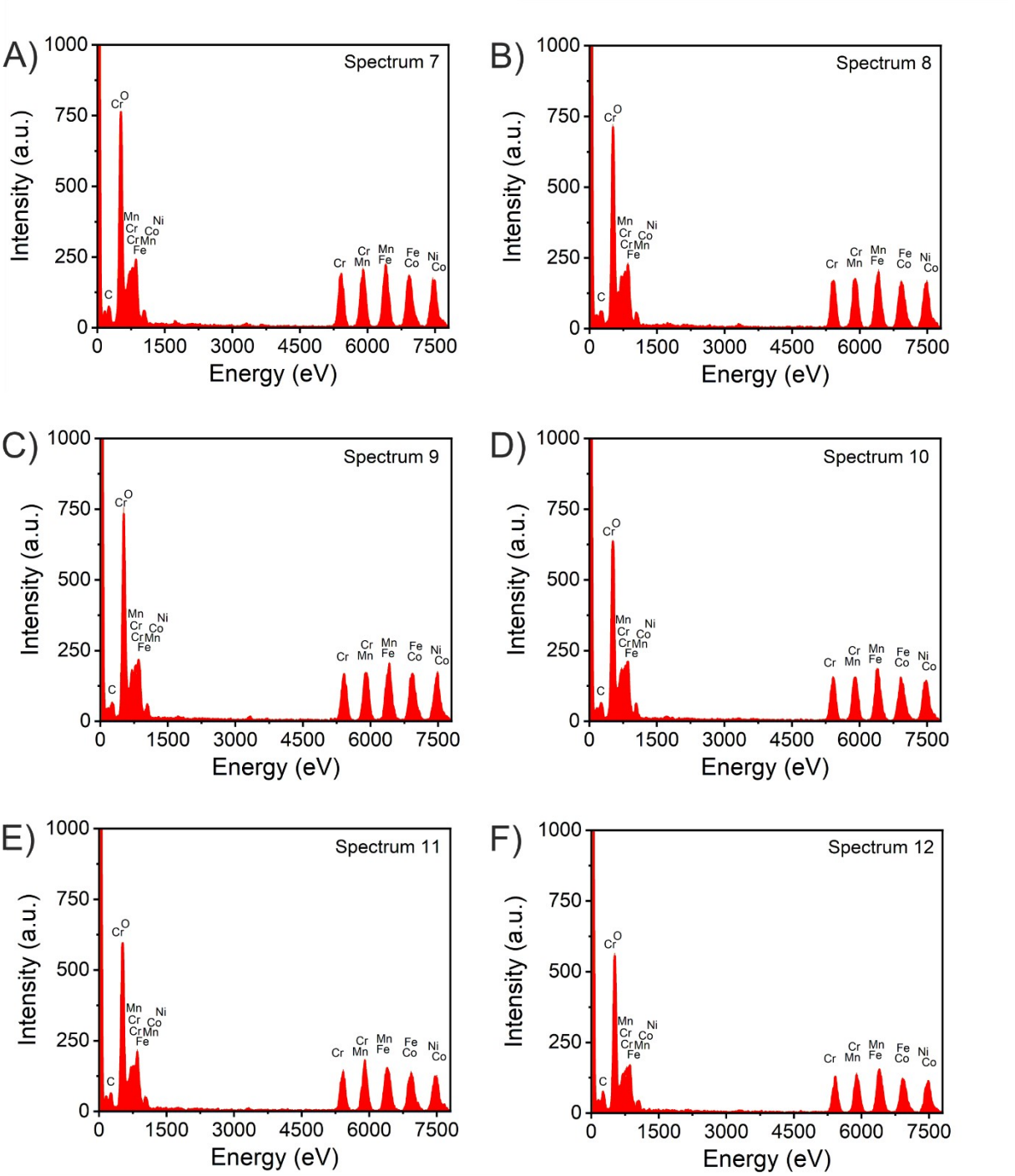

Figure S3. A)−F) STEM-based EDS spectra (7-12) conducted at six distinct spots of the HEO-400 thin films showing signals of all incorporated cations (Cr, Mn, Fe, Co, Ni) in near-equiatomic concentrations (± 5 % error) as well as carbon and oxygen.

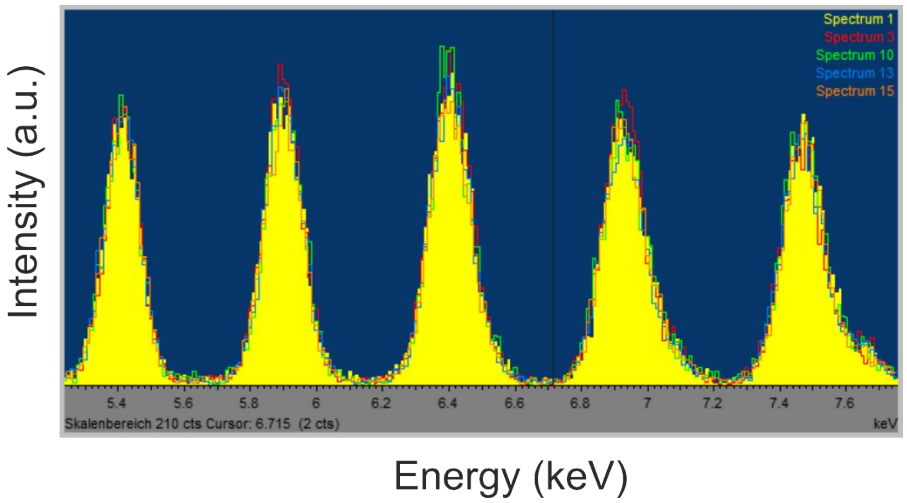

Figure S4. Overlaid EDS spectra (Spectrum 1, 3, 10, and 15 from Figure S3 and S4) showing signals of all incorporated cations (Cr, Mn, Fe, Co, Ni) and representing the homogenous distribution of all constituting transition metals in near-equiatomic concentrations (± 5 % error).

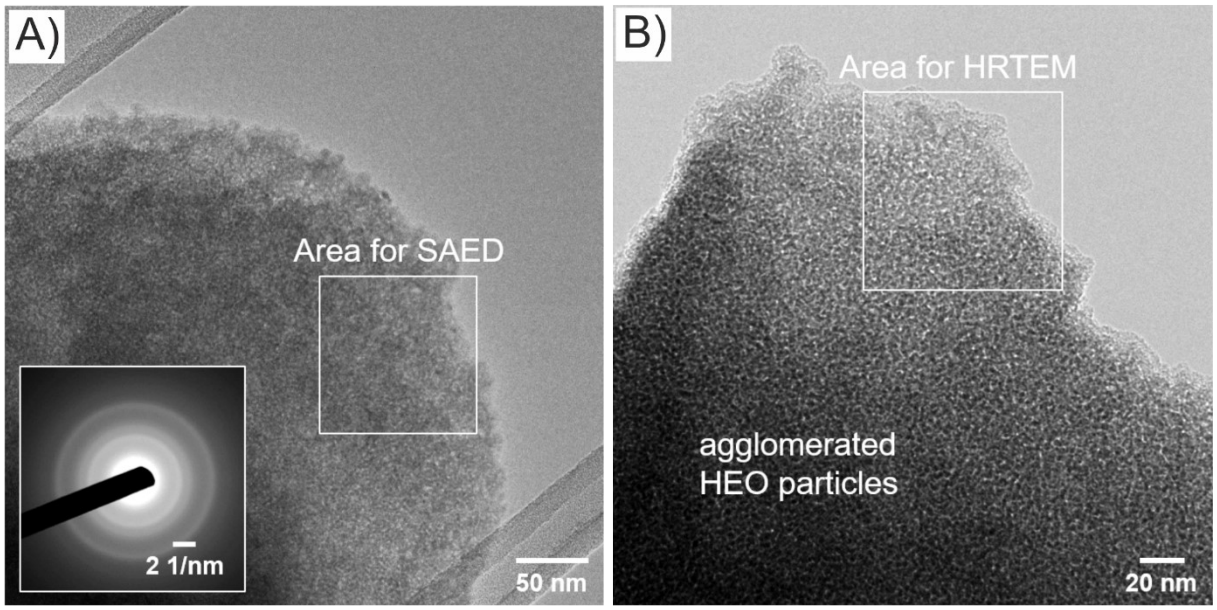

Figure S5. Bright-field TEM images of HEO-400-1h thin films with A) presenting the area for SAED analysis and B) the investigated area for the HRTEM image from Figure 1 E. The contrast in the TEM images indicates the nanoporous nature of the thin films.

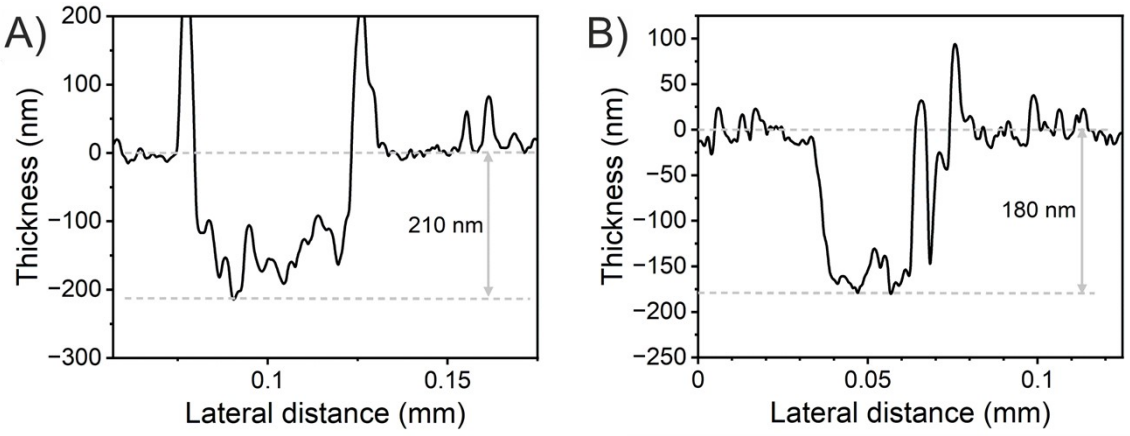

Figure S6. Profilometry of the A) HEO-400-10min and B) HEO-400-1h thin films presenting the determined thickness.

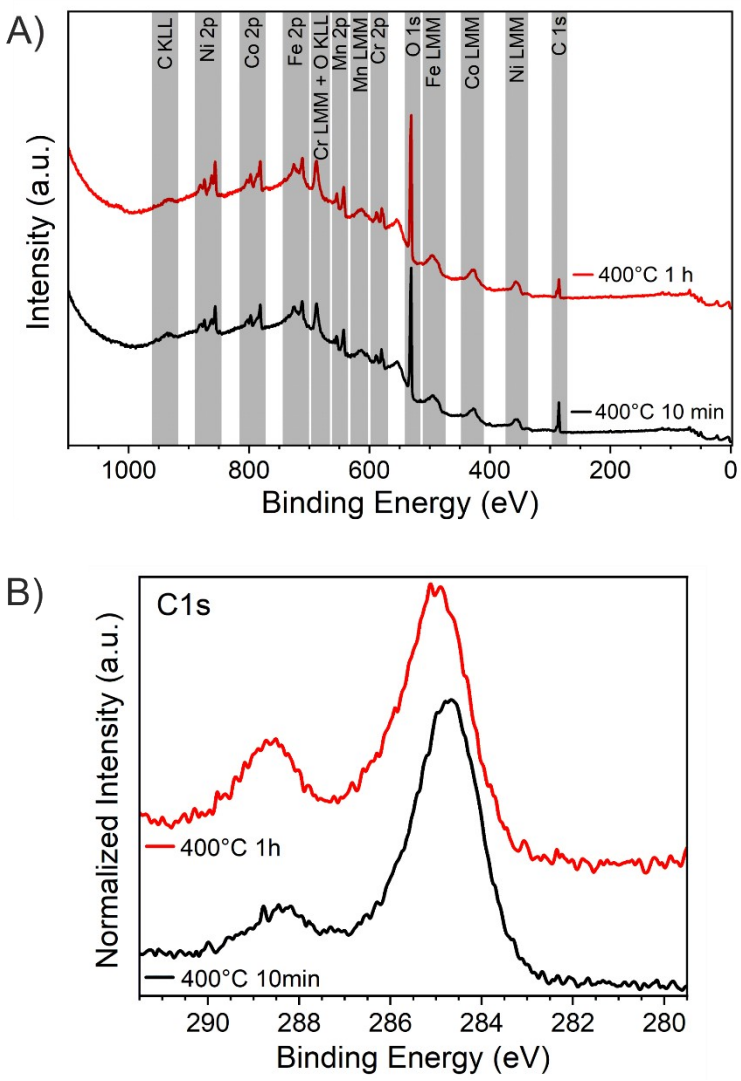

Figure S7. A) XP survey spectra and B) XP detail spectra of the C1 s emission lines of the HEO-400-10min (black) and HEO-400-1h (red) thin films.

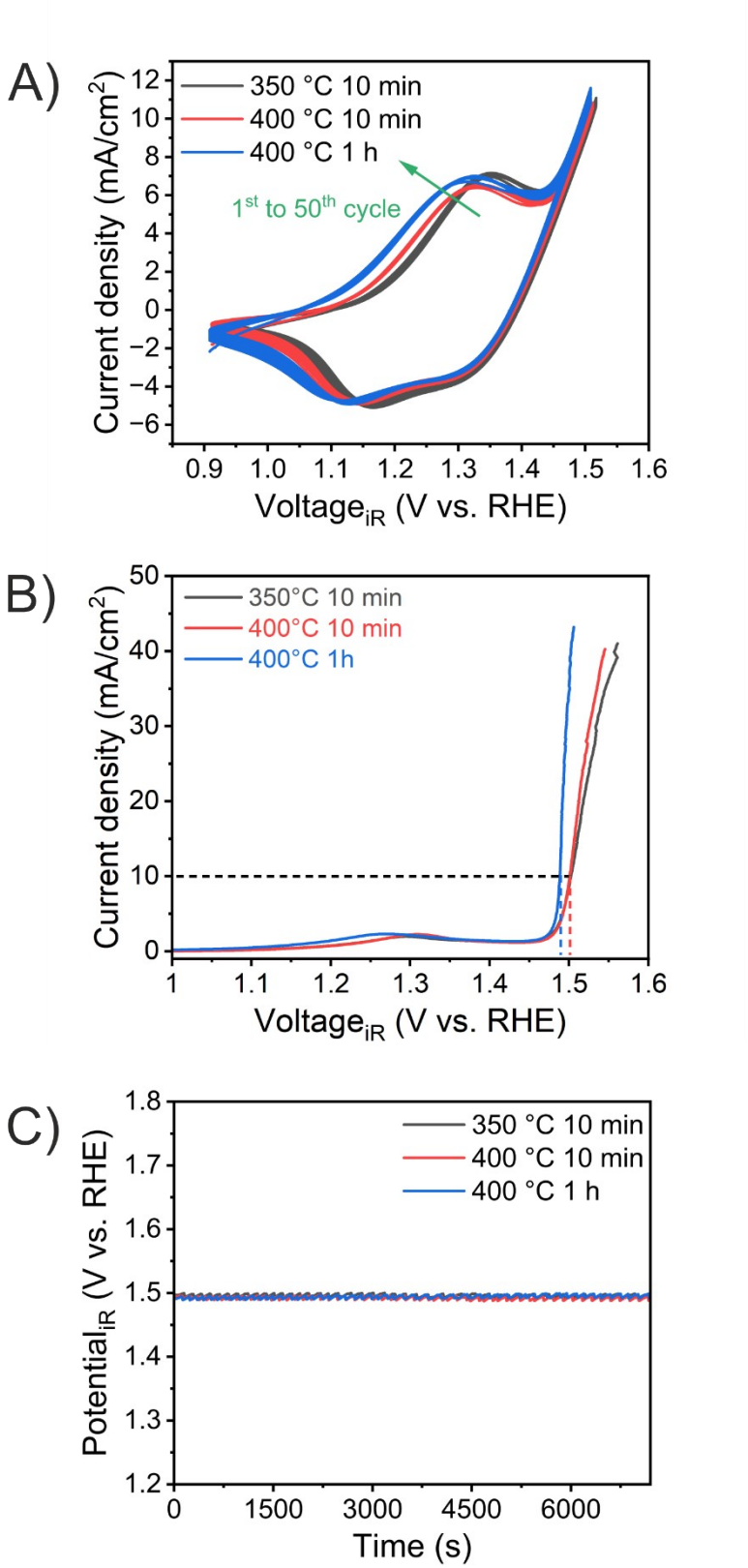

Figure S8. Electrochemical performance of HEO-350-10min (black), HEO-400-10min (red). and HEO-400-1h (blue): A) cyclic voltammetry curves, B) linear sweep voltammetry, and C) F) chronopotentiometry analysis performed at 10 mA/cm^2 for 2 hours. All experiments were conducted in 1 M KOH (pH ≈ 13.6).

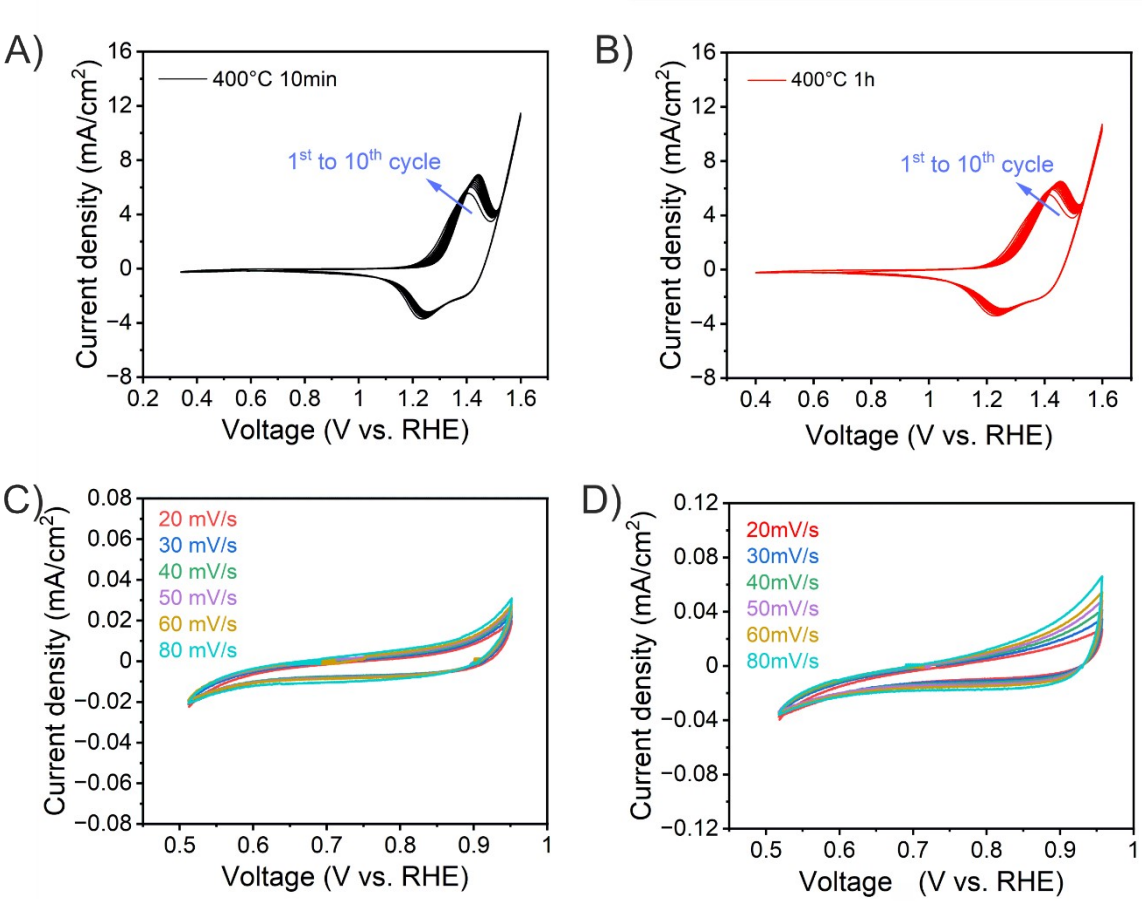

Figure S9. 10 consecutive CV scans of A) HEO-400-10min and B) HEO-400-1h thin films measured between 0.4 V and 1.6 V vs. RHE and collected at a scan rate of 50 mV/s. Scan rate-dependent CV curves of C) HEO-400-10min and D) HEO-400-1h thin films analyzed between 0.5 V and 0.95 V vs. RHE for various scan rates ranging from 20 mV/s to 80 mV/s.

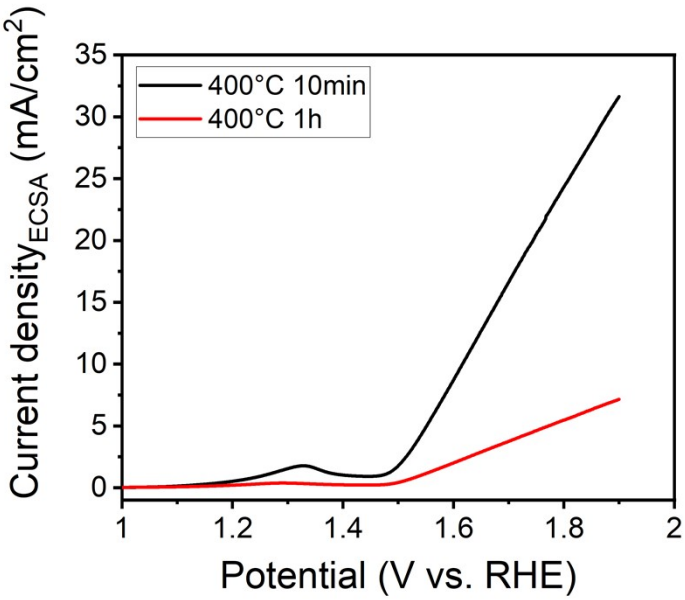

Figure S10. Linear sweep voltammetry nominated to the ECSA of HEO-400-10min and HEO-400-1h thin films, which were recorded with a scan rate of 10 mV/s in 1 M KOH.

Table S1: Tabular comparison of the atomic concentrations of the corresponding elements for HEO-400-10min and HEO-400-1h detected by EDS and analyzed on distinct spots at samples. Average values and standard deviations are presented.

	HEO-400-10min						**HEO-400-1h**					
EDS #	**Cr**	**Mn**	**Fe**	**Co**	**Ni**		**Cr**	**Mn**	**Fe**	**Co**	**Ni**	
	(at.-%)						**(at.-%)**					
1	2.5	2.2	2.5	2.6	2.5		1.9	1.8	2	2	2.2	
2	2.1	2	2.2	2.2	2.3		2	1.8	1.8	1.9	1.9	
3	2.3	2.1	2.1	2.2	2		1.8	1.7	1.8	1.9	1.6	
4	2.1	2.1	2.1	2.5	2.2		1.9	1.9	1.9	2.2	2.3	
5	1.6	1.6	1.6	1.8	1.6		1.6	1.4	1.6	1.8	1.7	
6	1.6	1.5	1.5	1.7	1.8		1.8	1.7	1.6	2	2	
7	1.9	1.4	1.8	2.1	1.8		2.3	2.1	2.3	2.4	2.6	
8	1.5	1.5	1.4	1.8	1.7							
9	1.8	1.7	1.7	2	2							
10	1.5	1.6	1.7	1.8	1.8							
Average	**1.89**	**1.77**	**1.86**	**2.07**	**1.97**		**1.90**	**1.77**	**1.86**	**2.03**	**2.04**	
Standard Deviation	**0.35**	**0.39**	**0.35**	**0.31**	**0.29**		**0.21**	**0.21**	**0.24**	**0.20**	**0.35**	

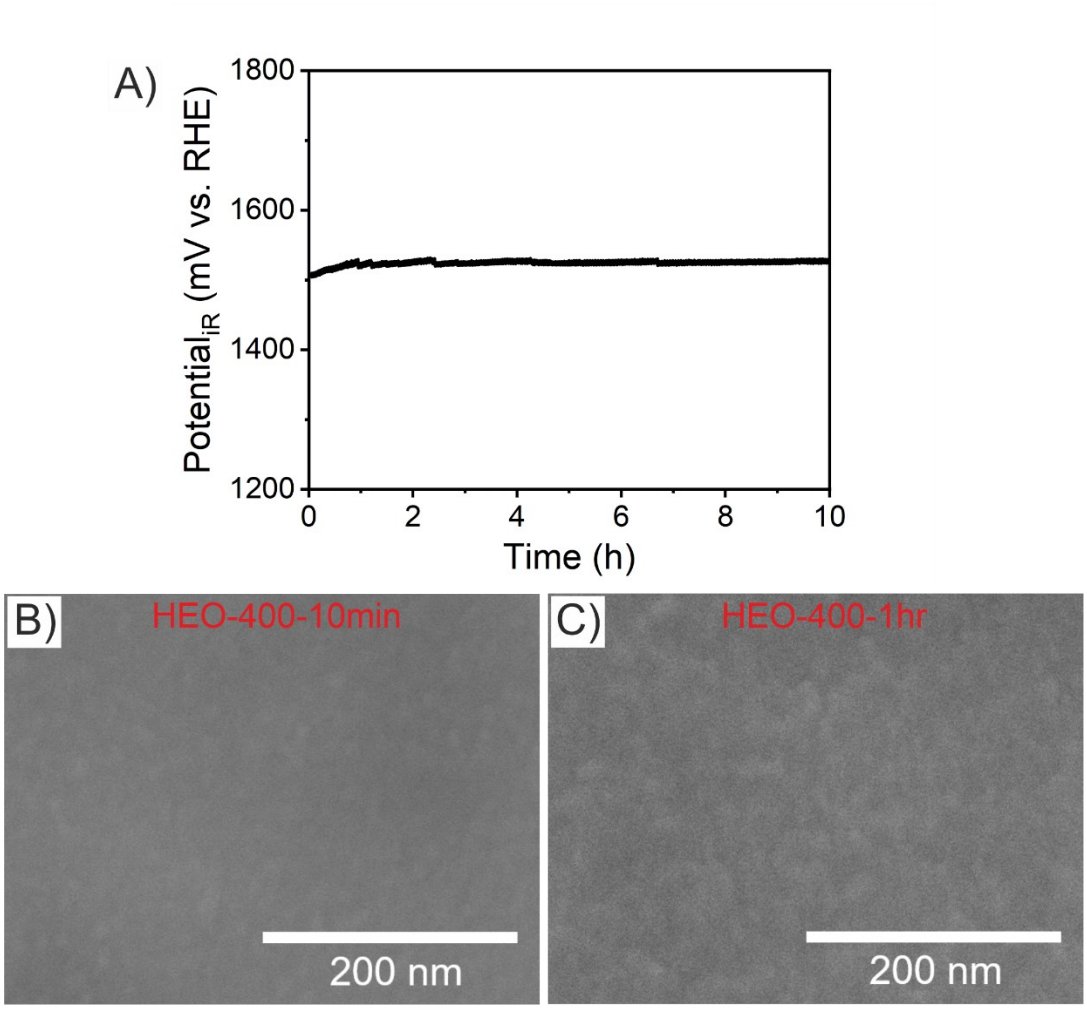

Figure S11. A) Chronopotentiometry analysis of nanoporous HEO-400-1h thin films performed at 10 mA/cm^2 for 10 hours. SEM images of B) HEO-400-10min and C) HEO-400-1h after chronopotentiometry investigations. All experiments were conducted in 1 M KOH (pH ≈ 13.6).

Table S2. Comparison of OER performances for cantor-alloy-based spinel high-entropy oxides investigated in alkaline solutions.

Catalyst composition	Electrolyte	Overpotential at 10mA/cm² (mV)	Stability	Tafel slope (mV/dec)	References
$(CoCrFeMnNi)_3O_4$	1.0 M KOH	220	500 mA/cm² for 1 h	100	3
$CoCrFeMnNiO_x$	1.0 M KOH	258	10 mA/cm² for 2h	40	This work
$(FeCoNiCrMn)_3O_4$	1.0 M KOH	288	10 mA/cm² for 95 h	60	4
$(CrMnFeCoNi)_3O_4$	1.0 M KOH	332	1.55 V_{RHE} for 20 h	55	5
$(CrMnFeCoNi)_3O_4$	1.0 M KOH	350	10 mA/cm² for 1 h	35	1
$(Cr_{23}Mn_{16}Fe_{17}Co_{27}Ni_{17})O_x$	1.0 M KOH	360	n.a.	n.a.	6

References

1 M. Einert, M. Mellin, N. Bahadorani, C. Dietz, S. Lauterbach and J. P. Hofmann, Mesoporous high-entropy oxide thin films: electrocatalytic water oxidation on high-surface-area spinel (Cr0. 2Mn0. 2Fe0. 2Co0. 2Ni0. 2) 3O4 electrodes, *ACS Applied Energy Materials*, 2022, **5**, 717–730.

2 C. C. L. McCrory, S. Jung, J. C. Peters and T. F. Jaramillo, Benchmarking Heterogeneous Electrocatalysts for the Oxygen Evolution Reaction, *Journal of the American Chemical Society*, 2013, **135**, 16977–16987.

3 B. Talluri, K. Yoo and J. Kim, High entropy spinel metal oxide (CoCrFeMnNi) 3O4 nanoparticles as novel efficient electrocatalyst for methanol oxidation and oxygen evolution reactions, *Journal of Environmental Chemical Engineering*, 2022, **10**, 106932.

4 C. Duan, X. Li, D. Wang, Z. Wang, H. Sun, R. Zheng and Y. Liu, Nanosized high entropy spinel oxide (FeCoNiCrMn) 3 O 4 as a highly active and ultra-stable electrocatalyst for the oxygen evolution reaction, *Sustainable Energy & Fuels*, 2022, **6**, 1479–1488.

5 Z. Sun, Y. Zhao, C. Sun, Q. Ni, C. Wang and H. Jin, High entropy spinel-structure oxide for electrochemical application, *Chemical Engineering Journal*, 2022, **431**, 133448.

6 V. Strotkötter, O. A. Krysiak, J. Zhang, X. Wang, E. Suhr, W. Schuhmann and A. Ludwig, Discovery of High-Entropy Oxide Electrocatalysts: From Thin-Film Material Libraries to Particles, *Chemistry of Materials*, 2022, **34**, 10291–10303.